Analytical Expressions for Multiobjective Optimization of Converter-Based DG Operation Under Unbalanced Grid Conditions

Masoud M. Shabestary, *Student Member, IEEE*, and Yasser Abdel-Rady I. Mohamed, *Senior Member, IEEE*

Abstract—Recently, riding through grid faults and supporting the grid voltage by using grid-connected converters (GCCs) have become major requirements reflected in the grid codes. This paper presents a novel reference current generation scheme with the ability to support the grid voltage by injecting a proper set of positive/negative active/reactive currents by using four controlling parameters. Analytical expressions are proposed to obtain the optimal values of these parameters under any grid voltage condition. The optimal performances can be obtained by achieving the following objectives: first, compliance with the phase voltage limits, second, maximized active and reactive power delivery, third, minimized fault currents, and fourth reduced oscillations on the active and reactive powers. These optimal behaviors bring significant advantages to emerging GCCs, such as increasing the efficiency, lowering the dc-link ripples, improving ac system stability, and avoiding equipment tripping. Simulation and experimental results verify the analytical results and the proposed expressions.

Index Terms—Grid faults, low-voltage ride-through (LVRT), power converters, reference-current generation.

NOMENCLATURE

V^+	Magnitude of positive-sequence of PCC Voltage.
V^-	Magnitude of negative-sequence of PCC Voltage.
n	Unbalance factor, V^-/V^+.
$g\,(b)$	Instantaneous conductance (susceptance).
$v_\perp$	Orthogonal voltage vector (90° leading from v).
$P^*(Q^*)$	Active (reactive) power reference command.
ω	Grid frequency.
$i_p^*\,(i_q^*)$	Active (reactive) current reference signal.
$P\,(Q)$	Average value of the active (reactive) power.
$\tilde{p}\,(\tilde{q})$	Active (reactive) power oscillatory terms.
$\tilde{p}_{s2}\,(\tilde{q}_{s2})$	Active (reactive) power oscillation terms oscillating by $\sin(2\omega t)$.
$\tilde{p}_{c2}\,(\tilde{q}_{c2})$	Active (reactive) power oscillation terms oscillating by $\cos(2\omega t)$.
$P_{s2}\,(P_{c2})$	Magnitude of $\tilde{p}_{s2}\,(\tilde{p}_{c2})$.
$Q_{s2}\,(Q_{c2})$	Magnitude of $\tilde{q}_{s2}\,(\tilde{q}_{c2})$.
X	System reactance.
R	System resistance.
$\tilde{p}_{\max}$	Magnitude of the oscillations on active power.
$\tilde{q}_{\max}$	Magnitude of the oscillations on reactive power.
$I_{\max}$	Maximum of three-phase currents under the fault.
I_{limit}	Imposed Limitation for $I_{\max}$.
$Q_{\max}$	Maximum allowable reactive power with respect to the I_{limit}.

I. INTRODUCTION

THE increasingly high penetration of renewable energy resources and distributed generation (DG) units into power systems has created serious stability concerns. Consequently, system planners have been developing rigorous requirements for grid-connected converters (GCCs) operation under abnormal grid conditions [1]–[3]. Accordingly, GCCs should not only withstand such disturbances and keep feeding the grid, but also provide voltage/frequency supports. The compliance of GCCs with these new requirements has been extensively studied in the literature, as, for instance, in [1]–[20]. In this regard, many control strategies for GCCs have been proposed in [13]–[20].

This paper uses, then modifies, the most advanced reference current generator (RCG) strategy (introduced in [3]), which can flexibly contain positive/negative and active/reactive currents. This RCG offers valuable voltage support services with two controlling parameters, k_p and k_q, balancing between the positive and negative sequences of the corresponding active and reactive currents. As well, the reference values for the active and reactive powers (P^* and Q^*) can be considered as other two reference values.

This paper initially presents detailed analytical expressions to characterize the performance of the applied RCG. These expressions are useful for engineers to design the control schemes of a GCC properly. Maximum oscillations on instantaneous active/reactive powers ($\tilde{p}_{\max}$ and $\tilde{q}_{\max}$) and the maximum phase currents ($I_{\max}$) are the three most important features of RCG strategies. The mathematical equations of $\tilde{p}_{\max}$, $\tilde{q}_{\max}$, and $I_{\max}$ for the applied RCG are calculated in this paper. The analytical study and the ideas proposed in this paper can also be expanded to other strategies.

As the main contribution, this paper proposes a new control scheme with analytical expressions capable of finding the optimal values for the controlling reference parameters (k_p, k_q, P^*, and Q^*) under any unbalanced voltage condition in order to achieve the following objectives:

1) minimized oscillations on the active and reactive powers;
2) boosted and semibalanced phase voltages of the point of common coupling (PCC); and
3) minimized inverter fault current.

To fully accomplish these objectives, the expressions of the boosted phase voltages, maximum oscillations on instantaneous active/reactive powers, and the maximum phase currents under the unbalanced conditions must be found.

As a second contribution, the maximum allowable support (MAS) is proposed to obtain the maximum allowable active or reactive powers which the converter can deliver to the grid under abnormal grid conditions (in order to support either the grid voltage or the grid frequency) without exceeding the maximum allowable instantaneous phase current limit, I_{limit}. The MAS control scheme aims to provide the maximum support for the grid voltage and/or frequency and simultaneously to respect the maximum limit of the phase currents imposed by the GCC rating. The mathematical equations of the MAS control schemes under various conditions (i.e., different fault types, various voltage dip characteristics, several system parameters, different operating points, etc.) are also obtained and presented in Section III. The proposed expressions are validated by various simulation and experimental test cases in Sections V and VI, which also verify the accuracy and effectiveness of the proposed control schemes.

II. MATHEMATICAL ASSESSMENT OF THE RCG STRATEGY

The total injected current by a GCC, i, can be written in terms of its active/reactive and positive/negative components as

$$i = i_p + i_q = i_p^+ + i_p^- + i_q^+ + i_q^- \tag{1}$$

where the vectors with superscripts "+"/"−" and subscripts "p"/"q" denote the positive/negative and active/reactive components, respectively. The reference positive/negative and active/reactive currents can be flexibly determined to provide the optimal operational performances of a GCC under various conditions, such as various unbalanced faults, different code requirements, and different line impedances. The total reference current can be formulated by using four components (positive/negative and active/reactive) as

$$i_p^+ = k_p \frac{P^*}{(V^+)^2} v^+ = K_p^+ v^+ \quad i_p^- = (1 - k_p) \frac{P^*}{(V^-)^2} v^- = K_p^- v^-$$

$$i_q^+ = k_q \frac{Q^*}{(V^+)^2} v_\perp^+ = K_q^+ v_\perp^+ \quad i_q^- = (1 - k_q) \frac{Q^*}{(V^-)^2} v_\perp^- = K_q^- v_\perp^-. \tag{2}$$

These four components provide four degrees of freedom which will be used in next sections to fulfill different objectives.

A. Mathematical Equations of Instantaneous Active/Reactive Power Oscillation Terms

In this section, the equations of $\tilde{p}_{\max}$ and $\tilde{q}_{\max}$ (under one-phase fault) are obtained based on the reference current of (2).

The detailed derivation of the instantaneous active power is provided in (3). A similar procedure can be applied to find the instantaneous reactive power:

$$p = v.\, i = (v^+ + v^-).(i^+ + i^-)$$

$$= \underbrace{v^+.\, i^+ + v^-.\, i^-}_{P} + \underbrace{v^+.\, i^- + v^-.\, i^+}_{\tilde{p}}$$

$$= v^+(K_p^+ v^+ + K_q^+ v_\perp^+) + v^-(K_p^- v^- + K_q^- v_\perp^-)$$
$$\quad + v^+(K_p^- v^- + K_q^- v_\perp^-) + v^-(K_p^+ v^+ + K_q^+ v_\perp^+)$$

$$= \underbrace{K_p^+ (V^+)^2 + K_p^- (V^-)^2}_{P} + \underbrace{(K_p^- + K_p^+) v^+ v^-}_{\tilde{p}_{c2}}$$

$$\quad + \underbrace{(K_q^- - K_q^+) v^+ v_\perp^-}_{\tilde{p}_{s2}}$$

$$= P - [P \times (1 - k_p)/n + P \times k_p \times n] \, \cos(2\omega t)$$
$$\quad - [Q \times (1 - k_q)/n - Q \times k_q \times n] \sin(2\omega t) \tag{3}$$

$$q = v_\perp.\, i = (v_\perp^+ + v_\perp^-).(i^+ + i^-)$$

$$= \underbrace{v_\perp^+.\, i^+ + v_\perp^-.\, i^-}_{Q} + \underbrace{v_\perp^+.\, i^- + v_\perp^-.\, i^+}_{\tilde{q}} = Q + \tilde{q}_{s2} + \tilde{q}_{c2}$$

$$= v_\perp^+(K_p^+ v^+ + K_q^+ v_\perp^+) + v_\perp^-(K_p^- v^- + K_q^- v_\perp^-)$$
$$\quad + v_\perp^+(K_p^- v^- + K_q^- v_\perp^-) + v_\perp^-(K_p^+ v^+ + K_q^+ v_\perp^+)$$

$$= \underbrace{K_q^+ (V^+)^2 + K_q^- (V^-)^2}_{Q} + \underbrace{(K_p^- - K_p^+) v_\perp^+ v^-}_{\tilde{q}_{s2}}$$

$$\quad + \underbrace{(K_q^- + K_q^+) v_\perp^+ v_\perp^-}_{\tilde{q}_{c2}}$$

$$= Q + [P \times (1 - k_p)/n - P \times k_p \times n] \, \sin(2\omega t)$$
$$\quad - [Q \times (1 - k_q)/n + Q \times k_q \times n] \cos(2\omega t). \tag{4}$$

The ability to analytically calculate the maximum power oscillations, i.e., $\tilde{p}_{\max}$ and $\tilde{q}_{\max}$, in terms of the scalar parameters (i.e., P, Q, k_p, k_q, and n) is very useful for proper control of a GCC. Therefore, the expressions of $\tilde{p}_{\max}$ and $\tilde{q}_{\max}$ can be obtained by using (3) and (4) as

$$\tilde{p}_{\max}$$
$$= \sqrt{P^2 [k_p n + (1 - k_p)\, n^{-1}]^2 + Q^2 [k_q n - (1 - k_q)\, n^{-1}]^2} \tag{5}$$

$$\tilde{q}_{\max}$$
$$= \sqrt{Q^2 [k_q n + (1 - k_q)\, n^{-1}]^2 + P^2 [k_p n - (1 - k_p)\, n^{-1}]^2}. \tag{6}$$

In this paper, these equations are used to minimize the oscillations on the instantaneous active and reactive powers.

B. Mathematical Expressions of Maximum Instantaneous Phase Currents

The voltage under a single-phase unbalanced fault can be simplified as [3], [13]

$$v^+ = \begin{bmatrix} v_\alpha^+ \\ v_\beta^+ \end{bmatrix} = \begin{bmatrix} V^+ \cos(\omega t) \\ V^+ \sin(\omega t) \end{bmatrix}$$

$$v^- = \begin{bmatrix} v_\alpha^- \\ v_\beta^- \end{bmatrix} = \begin{bmatrix} -V^- \cos(\omega t) \\ V^- \sin(\omega t) \end{bmatrix} \tag{7}$$

$$v_\perp^+ = \begin{bmatrix} v_{\perp\alpha}^+ \\ v_{\perp\beta}^+ \end{bmatrix} = \begin{bmatrix} -V^+ \sin(\omega t) \\ V^+ \cos(\omega t) \end{bmatrix}$$

$$v_\perp^- = \begin{bmatrix} v_{\perp\alpha}^- \\ v_{\perp\beta}^- \end{bmatrix} = \begin{bmatrix} -V^- \sin(\omega t) \\ -V^- \cos(\omega t) \end{bmatrix}. \tag{8}$$

By using (7) and (8) in (1) and (2), the injected current under the fault can be rewritten in the $\alpha\beta$ reference frame as

$$\begin{bmatrix} i_\alpha \\ i_\beta \end{bmatrix} = \begin{bmatrix} i_{p,\alpha}^+ \\ i_{p,\beta}^+ \end{bmatrix} + \begin{bmatrix} i_{p,\alpha}^- \\ i_{p,\beta}^- \end{bmatrix} + \begin{bmatrix} i_{q,\alpha}^+ \\ i_{q,\beta}^+ \end{bmatrix} + \begin{bmatrix} i_{q,\alpha}^- \\ i_{q,\beta}^- \end{bmatrix}$$

$$= K_p^+ \begin{bmatrix} v_\alpha^+ \\ v_\beta^+ \end{bmatrix} + K_p^- \begin{bmatrix} v_\alpha^- \\ v_\beta^- \end{bmatrix} + K_q^+ \begin{bmatrix} -v_\beta^+ \\ v_\alpha^+ \end{bmatrix} + K_q^- \begin{bmatrix} -v_\beta^- \\ v_\alpha^- \end{bmatrix}$$

$$= \begin{bmatrix} \left[K_p^+ V^+ - K_p^- V^-\right]\cos(\omega t) - \left[K_q^+ V^+ + K_q^- V^-\right]\sin(\omega t) \\ \left[K_p^+ V^+ + K_p^- V^-\right]\sin(\omega t) + \left[K_q^+ V^+ - K_q^- V^-\right]\cos(\omega t) \end{bmatrix}. \tag{9}$$

The $\alpha\beta$ currents of (9) are transformed into the *abc* currents by the transformation matrix in the following:

$$\begin{bmatrix} i_a \\ i_b \\ i_c \end{bmatrix} = \begin{bmatrix} 1 & 0 \\ -\frac{1}{2} & \frac{\sqrt{3}}{2} \\ -\frac{1}{2} & -\frac{\sqrt{3}}{2} \end{bmatrix} \cdot \begin{bmatrix} i_\alpha \\ i_\beta \end{bmatrix} \rightarrow$$

$$\begin{bmatrix} |i_a| \\ |i_b| \\ |i_c| \end{bmatrix} = \begin{bmatrix} |i_\alpha| \\ |-\frac{1}{2}i_\alpha + \frac{\sqrt{3}}{2}i_\beta| \\ |\frac{1}{2}i_\alpha + \frac{\sqrt{3}}{2}i_\beta| \end{bmatrix}. \tag{10}$$

Therefore, the maximum currents in each phase can be obtained as

$$\begin{bmatrix} I_{\max-a}^2 \\ I_{\max-b}^2 \\ I_{\max-c}^2 \end{bmatrix} = \begin{bmatrix} (K_1)^2 + (K_2)^2 \\ \left(-\frac{1}{2}K_1 + \frac{\sqrt{3}}{2}K_4\right)^2 + \left(\frac{1}{2}K_2 + \frac{\sqrt{3}}{2}K_3\right)^2 \\ \left(-\frac{1}{2}K_1 - \frac{\sqrt{3}}{2}K_4\right)^2 + \left(\frac{1}{2}K_2 - \frac{\sqrt{3}}{2}K_3\right)^2 \end{bmatrix}$$

where

$$\begin{cases} K_1 = K_p^+ V^+ - K_p^- V^- = \frac{P}{V^-}\left((n+1)k_p - 1\right) \\ K_2 = K_q^+ V^+ + K_q^- V^- = \frac{Q}{V^-}\left((n-1)k_q + 1\right) \\ K_3 = K_p^+ V^+ + K_p^- V^- = \frac{P}{V^-}\left((n-1)k_p + 1\right) \\ K_4 = K_q^+ V^+ - K_q^- V^- = \frac{Q}{V^-}\left((n+1)k_q - 1\right) \end{cases}. \tag{11}$$

Then, the maximum phase current under the fault can be found by

$$I_{\max} = \max\left(I_{\max-a},\ I_{\max-b},\ I_{\max-c}\right). \tag{12}$$

III. PROPOSED OPTIMAL SUPPORT SCHEMES

The optimized operation of a converter-interfaced DG power plant is proposed under unbalanced grid conditions. Applying the proposed control schemes provides the optimal performances in terms of riding through abnormal conditions and assisting the voltage and frequency stability/improvement where the important constraint of the maximum phase current, I_{limit}, is not exceeded.

This paper initially proposes five optimal operation strategies in this section:
1) minimized active power oscillation;
2) minimized reactive power oscillation;
3) minimized fault current;
4) maximum allowable active power injection; and
5) maximum allowable reactive power injection.

In the next section, an advanced strategy is also proposed which not only provides the maximum allowable active power injection, but also regulates the phase voltages within the desired limits.

A. Minimum Oscillations on the Instantaneous Active Power (MOP)

By taking the derivative of (5) in terms of k_p and k_q, and finding the extreme point by enforcing the derivatives to be zero, the following expression can be obtained for the minimum oscillations on the instantaneous active power:

$$\tilde{p}_{\max} \text{ is minimum when} \quad \begin{cases} k_p = 1/\left(1-n^2\right) \\ k_q = 1/\left(1+n^2\right) \end{cases}. \tag{13}$$

For an efficient power delivery, the k_p and k_q values are allowed to be only between 0 and 1 [14]–[20]. Because (13) gives a k_p value greater than 1, it can be changed to $k_p = 1$. In this case, only positive sequence active currents will be injected while the reactive currents will contain both positive and negative components based on $1/(1+n^2)$. However, k_p can be set to be $1/(1-n^2)$, as (13), in certain applications when minimizing the active power oscillations is critical. To improve the MOP strategy, P^* or Q^* can be obtained by using the proposed MAP or MAQ expressions, presented in Sections III-D and III-E, respectively. Therefore, the objectives of both strategies, i.e., MOP and MAS, can be simultaneously accomplished.

B. Minimum Oscillations on the Instantaneous Reactive Power (MOQ)

Calculating the minimum of (6) results in finding the following expressions for k_p and k_q:

$$\tilde{q}_{\max} \text{ is minimum when} \quad \begin{cases} k_p = 1/\left(1+n^2\right) \\ k_q = 1/\left(1-n^2\right) \end{cases}. \tag{14}$$

As stated earlier, the k_p and k_q values are allowed to be only between 0 and 1. Therefore, $k_q = 1$ is used to reduce the oscillations on Q, except in applications in which minimizing the reactive power oscillations is critical. Similarly, MOQ can also be combined with MAS strategies to achieve both objectives.

C. Minimum Fault Current (MFC)

To obtain the MFC, (11) should be considered. According to (11) and (12), the maximum instantaneous phase current can be one of the three expressions for the three phases. For the proposed MFC scheme, the reference values for the active and reactive powers can be determined from the operating mode controllers (either *PV* or *PQ* modes) or grid code requirements. Also, the value of k_q can be obtained from the voltage support scheme (VSS) introduced in the Section IV. Therefore, the minimum point of each expression of (11) should be obtained by taking their derivatives with respect to k_p

$$
\begin{aligned}
I_{a-\min} &\Rightarrow k_{p,a} = \frac{1}{n+1} \\[2mm]
I_{b-\min} &\Rightarrow k_{p,b} = \frac{P \times (2-n) + \sqrt{3}nQ \times (2k_q - 1)}{2P \times (n^2 - n + 1)} \\[2mm]
I_{c-\min} &\Rightarrow k_{p,c} = \frac{P \times (2-n) - \sqrt{3}nQ \times (2k_q - 1)}{2P \times (n^2 - n + 1)}.
\end{aligned}
\tag{15}
$$

However, the conditions in (15) cannot fully ensure that the obtained $k_{p,i}$ will always minimize $I_{\max}$ in (12) because these equations minimize only their corresponding currents, i.e., $I_{\max-a}$, $I_{\max-b}$, and $I_{\max-c}$. Therefore, in addition to the three k_ps obtained in (15), three other k_ps should be considered in order to find the optimum k_p. Two of these k_ps are the intersections of the magnitude curve of $I_a(k_p)$ with the magnitude curves of $I_b(k_p)$ and $I_c(k_p)$. Therefore, the equations of I_a and I_b, presented in (11), are taken to be equal to find $k_{p,ab}$. Similarly, the equations of I_a and I_c, given in (11), are set to be equal to find $k_{p,ac}$:

$$
I_a(k_p) = I_b(k_p) \Rightarrow k_{p,ab} = \frac{-b + \sqrt{b^2 - 4ac}}{2a}
$$

$$
\begin{cases}
a = 3nP^2 \\
b = -3nP^2 + \sqrt{3}nPQ(2k_q - 1) \\
c = 3nk_qQ^2(1 - k_q) - \sqrt{3}nPQk_q
\end{cases}
$$

$$
I_a(k_p) = I_c(k_p) \Rightarrow k_{p,ac} = \frac{-b + \sqrt{b^2 - 4ac}}{2a}
$$

$$
\begin{cases}
a = 3nP^2 \\
b = -3nP^2 - \sqrt{3}nPQ(2k_q - 1) \\
c = 3nk_qQ^2(1 - k_q) + \sqrt{3}nPQk_q
\end{cases}
\tag{16}
$$

Because k_p is bounded to 1, $k_{p,1} = 1$ should also be considered to find the minimum phase currents and optimal k_p value, i.e., $I_{\max,opt}$ and $k_{p,opt}$. Therefore, the three-phase currents are calculated by using (11) for six possible k_ps in order to find the minimum $I_{\max}$, i.e., $I_{\max,opt}$. The proposed

procedure, which is based on the six introduced k_ps, is better understood by sketching the magnitude curves of the *abc* currents with respect to k_p under different fault conditions, as illustrated in Fig. 1. This paper proposes that the optimal k_p value, i.e., $k_{p,opt}$, can be calculated under any operating and fault condition for any *P*, *Q*, V^+, and V^- values.

D. Maximum Allowable Active Power Delivery (MAP)

The MAP strategy is also proposed in this paper. Applying the MAP control scheme provides the maximum power to the grid and simultaneously respects the current thermal limitations while riding through abnormal conditions and assisting the frequency stability/improvement. Therefore, this section presents the required equations of P_{MAP} for faulted conditions based on the calculated $I_{\max}$ expressions of (11) in Section II.

The equations for the maximum allowable active power injection should be obtained so that they guarantee that none of the phase currents under the abnormal condition passes the predetermined limits, I_{limit}. In this strategy, the reference value for Q is determined either by the operating condition or grid code requirements for severe low voltages. By using the $I_{\max}$ equations of (11), P_{MAP}^* can be obtained. For example, the first expression in (11) gives

$$
I_{\max-a}^2 = (K_1)^2 + (K_2)^2 = \left(\frac{P}{V^-} \left((n+1)k_p - 1 \right) \right)^2
$$

$$
+ \left(\frac{Q}{V^-} \left((n-1)k_q + 1 \right) \right)^2
$$

$$
\Rightarrow \left(\frac{P}{V^-} \left((n+1)k_p - 1 \right) \right)
$$

$$
= \sqrt{I_{\max-a}^2 - \left(\frac{Q}{V^-} \left((n-1)k_q + 1 \right) \right)^2}
$$

$$
\Rightarrow P = \frac{V^- \times \sqrt{I_{\max-a}^2 - \left(\frac{Q}{V^-} \left((n-1)k_q + 1 \right) \right)^2}}{\left((n+1)k_p - 1 \right)}.
\tag{17}
$$

Similarly, the other two expressions of (11) can also be manipulated to obtain all three possible active power values as

$$
\begin{bmatrix} P_1 \\ P_2 \\ P_3 \end{bmatrix} =
\begin{bmatrix}
\dfrac{V^- \sqrt{I_{\max}^2 - K_2^2}}{k_p n + k_p - 1} \\[3mm]
\dfrac{-b + \sqrt{b^2 - 4ac}}{2a} \\[3mm]
\dfrac{b + \sqrt{b^2 - 4ac}}{2a}
\end{bmatrix}
$$

$$
\begin{cases}
a = \dfrac{3}{V^-}(k_p(n-1) + 1)^2 + \dfrac{1}{V^-}(k_p(n+1) - 1)^2 \\[2mm]
b = 2\sqrt{3}\left[\dfrac{K_4}{V^-}(k_p(n+1) - 1) - \dfrac{K_2}{V^-}(k_p(n-1) + 1) \right] \\[2mm]
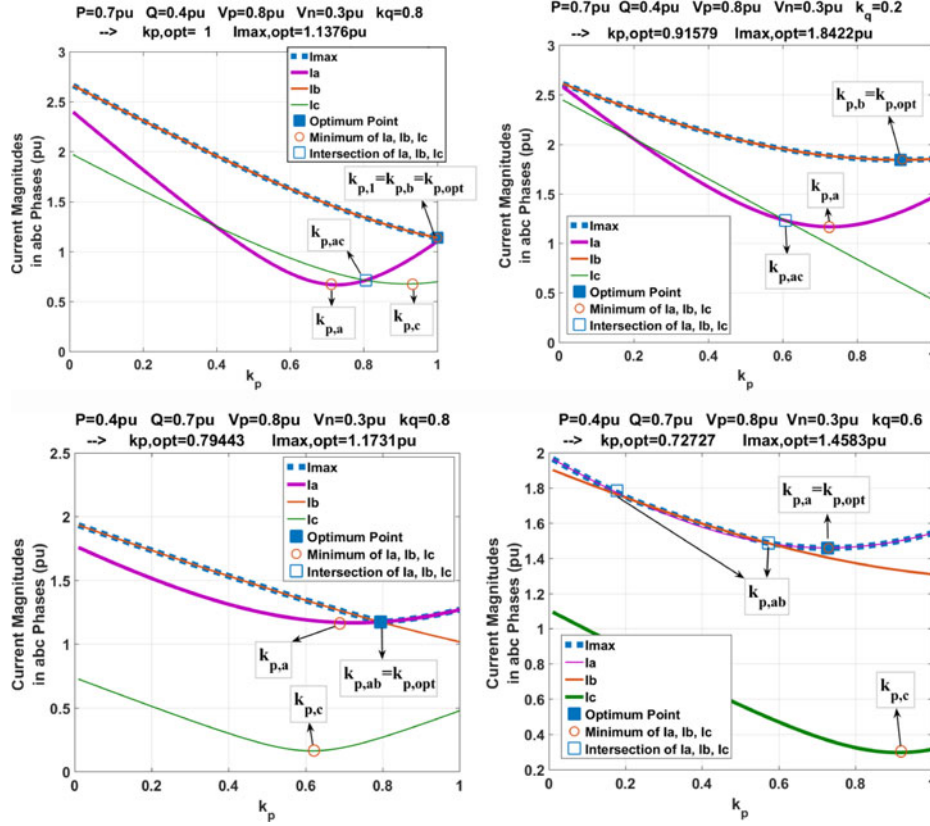c = K_2^2 + 3K_4^2 - 4I_{\max}^2
\end{cases}
\tag{18}
$$

Fig. 1.   Magnitude curves of *abc* currents with respect to k_p.

To have all of the three-phase currents of (11) lower than the preset I_{limit} value, P^*_{MAP} should comply with

$$P^*_{\text{MAP}} = \min(P_1, P_2, P_3). \tag{19}$$

E. Maximum Allowable Reactive Power Delivery (MAQ)

Similarly, the maximum allowable reactive power reference value, Q^*_{MAQ}, can be obtained such that all phase currents (under any abnormal condition) remain bounded with the predetermined current limitation, I_{limit}. Here, the reference value of P is determined by other controllers in the GCC (e.g., by maximum power point tracking), and the Q^*_{MAQ} expressions can be obtained by using the $I_{\max}$ equations of (11). For example, the first current expression in (11) provides Q_1 as

$$I^2_{\max-a} = (K_1)^2 + (K_2)^2 = \left(\frac{P}{V^-}((n+1)k_p - 1)\right)^2$$
$$+ \left(\frac{Q}{V^-}((n-1)k_q + 1)\right)^2$$

$$[-4pt] \Rightarrow \left(\frac{Q}{V^-}((n-1)k_q + 1)\right)$$

$$= \sqrt{I^2_{\max-a} - \left(\frac{P}{V^-}((n+1)k_p - 1)\right)^2}$$

$$[-4pt] \Rightarrow Q_1 = \frac{V^- \times \sqrt{I^2_{\max-a} - \left(\frac{P}{V^-}((n+1)k_p - 1)\right)^2}}{((n-1)k_q + 1)}. \tag{20}$$

Similarly, the other two expressions of (11) can also be used to find all three possible reactive power reference values as

$$\begin{bmatrix} Q_1 \\ Q_2 \\ Q_3 \end{bmatrix} = \begin{bmatrix} \dfrac{V^- \sqrt{I^2_{\max} - K_1^2}}{k_q n - k_q + 1} \\ \dfrac{-b + \sqrt{b^2 - 4ac}}{2a} \\ \dfrac{b + \sqrt{b^2 - 4ac}}{2a} \end{bmatrix}$$

$$\begin{cases} a = \dfrac{3}{V^-}(k_q(n+1) - 1)^2 + \dfrac{1}{V^-}(k_q(n-1) + 1)^2 \\ b = 2\sqrt{3}\left[\dfrac{K_3}{V^-}(k_q(n-1) + 1) - \dfrac{K_1}{V^-}(k_q(n+1) - 1)\right] \cdot \\ c = K_1^2 + 3K_3^2 - 4I^2_{\max} \end{cases} \tag{21}$$

Finally, in order to satisfy that the maximum of I_a, I_b, and I_c is less than or equal to I_{limit}, Q^*_{MAQ} can be obtained as

$$Q^*_{\text{MAQ}} = \min(Q_1, Q_2, Q_3). \tag{22}$$

IV. VOLTAGE SUPPORT SCHEME AND MAXIMUM ALLOWABLE ACTIVE POWER DELIVERY (VSS-MAP)

Supporting the PCC voltage by using DG units is another important objective, and it is considered in this paper. If the DG plant rated power and the grid impedance are not small, then, under the moderate sags, the three-phase voltages can be regulated at the desired range between $V_{\min}$ and $V_{\max}$. In [15],

the proposed scheme has been applied to a static synchronous compensator, where the reference current consists of only the reactive power. The primary requirement in the voltage support is to avoid the overvoltage and undervoltage at the PCC whenever possible. However, a proper solution can be found in this range to satisfy other objectives as well. Unlike [15], this paper considers the active components of the current. Complying with the voltage limits during unbalanced grid faults can be formulated as

$$V_{abc-\max} = \max\{V_a, V_b, V_c\} \le V_{\max}$$
$$V_{abc-\min} = \min\{V_a, V_b, V_c\} \ge V_{\min} \qquad (23)$$

where $V_{\max}$ and $V_{\min}$ are thresholds for the upper and lower safety limits according to the grid codes, which are set to 1.1 per unit (p.u.) and 0.9 p.u. here, respectively. To meet these limits, a combination of positive/negative and active/reactive powers (P^+, P^-, Q^+, and Q^-) should be injected into an inductive or resistive grid to support the grid voltage. These four reference values (P^+, P^-, Q^+, and Q^-) should be properly found so that the maximum phase voltage does not exceed $V_{\max}$, and the minimum phase voltage is kept at (or above) $V_{\min}$. Therefore, the controlling reference parameters can be analytically determined to properly support the voltage in an online manner. The PCC VSS can be extracted as a function of the grid voltage and the injected positive/negative currents. The mathematical expressions of the PCC voltage in terms of the injected active/reactive powers are as follows:

$$v = v^+ + v^- = \begin{bmatrix} v_\alpha^+ + v_\alpha^- \\ v_\beta^+ + v_\beta^- \end{bmatrix}$$

$$= \begin{bmatrix} v_{g\alpha}^+ + v_{g\alpha}^- + L_g \dfrac{d(i_\alpha^+ + i_\alpha^-)}{dt} + R_g(i_\alpha^+ + i_\alpha^-) \\ v_{g\beta}^+ + v_{g\beta}^- + L_g \dfrac{d(i_\beta^+ + i_\beta^-)}{dt} + R_g(i_\beta^+ + i_\beta^-) \end{bmatrix}. \qquad (24)$$

Applying (7)–(9) and (11) in (24) gives the following:

$$\begin{bmatrix} (V^+ - V^-)\cos(\omega t) \\ (V^+ + V^-)\sin(\omega t) \end{bmatrix} = \begin{bmatrix} (V_g^+ - V_g^-)\cos(\omega t - \delta) \\ (V_g^+ + V_g^-)\sin(\omega t - \delta) \end{bmatrix}$$
$$+ \begin{bmatrix} \omega L_g(-K_1\sin(\omega t) + K_2\cos(\omega t)) \\ \omega L_g(-K_3\sin(\omega t) + K_4\cos(\omega t)) \end{bmatrix}$$
$$+ \begin{bmatrix} R_g(K_1\cos(\omega t) + K_2\sin(\omega t)) \\ R_g(K_3\cos(\omega t) + K_4\sin(\omega t)) \end{bmatrix}. \qquad (25)$$

In practical applications, δ is small and can be neglected for the sake of simplicity in the analytical solution. Then, the positive and negative components of (25) can be separated as

$$\begin{bmatrix} V^+ \\ V^- \end{bmatrix} - \begin{bmatrix} V_g^+ \\ V_g^- \end{bmatrix} = \begin{bmatrix} \omega L_g I_q^+ \\ -\omega L_g I_q^- \end{bmatrix} + \begin{bmatrix} R_g I_p^+ \\ R_g I_p^- \end{bmatrix}. \qquad (26)$$

On the other hand, the magnitudes of the phase voltages are obtained in terms of the voltage magnitudes of positive and negative sequences by using following expressions:

$$\begin{cases} V_a = \sqrt{(V^+)^2 + (V^-)^2 + 2(V^+)(V^-)\cos(\gamma)} \\ V_b = \sqrt{(V^+)^2 + (V^-)^2 + 2(V^+)(V^-)\cos\left(\gamma - \dfrac{2\pi}{3}\right)} \\ V_c = \sqrt{(V^+)^2 + (V^-)^2 + 2(V^+)(V^-)\cos\left(\gamma + \dfrac{2\pi}{3}\right)} \end{cases}. \qquad (27)$$

From (27), the maximum and minimum phase voltages can be determined simply by [14]–[15]

$$V_{abc-\min} = \min(V_a, V_b, V_c)$$
$$= \sqrt{(V^+)^2 + (V^-)^2 + 2(V^+)(V^-)\lambda_{\min}}$$
$$V_{abc-\max} = \max(V_a, V_b, V_c)$$
$$= \sqrt{(V^+)^2 + (V^-)^2 + 2(V^+)(V^-)\lambda_{\max}} \qquad (28)$$

where

$$\lambda_{\min} = \min\left(\cos(\gamma), \cos\left(\gamma - \dfrac{2\pi}{3}\right), \cos\left(\gamma + \dfrac{2\pi}{3}\right)\right)$$
$$\lambda_{\max} = \max\left(\cos(\gamma), \cos\left(\gamma - \dfrac{2\pi}{3}\right), \cos\left(\gamma + \dfrac{2\pi}{3}\right)\right). \qquad (29)$$

Then, the reference values for the maximum and minimum phase voltages can be determined so that the phase voltages are regulated within the explained thresholds. This process can be accomplished by setting the reference values as [15]

$$V_{abc-\min}^* = V_{\min}$$
$$V_{abc-\max}^* = \min(V_{\max}, V_{\min} + V_{abc-\max} - V_{abc-\min}). \qquad (30)$$

After finding the proper $V_{abc-\min}^*$ and $V_{abc-\max}^*$ by using (30) and applying them in (28), the reference values for the V_{ref}^+ and V_{ref}^- can be calculated as equations (31) and (32) as shown on the bottom of the next page [15].

By using (31) and (32), the reference values for the desired positive and negative sequences of the voltage are obtained. Then, V^+ and V^- in (26) are replaced with the reference values obtained from (31) and (32). Moreover, V_g^+ and V_g^- can be estimated from the PCC measurements. Therefore, (26) can be rewritten as

$$\begin{bmatrix} \Delta V_{ref}^+ \\ \Delta V_{ref}^- \end{bmatrix} = \begin{bmatrix} \omega L_g I_q^+ \\ -\omega L_g I_q^- \end{bmatrix} + \begin{bmatrix} R_g I_p^+ \\ R_g I_p^- \end{bmatrix}. \qquad (33)$$

Now, (33) can be solved by determining four current components (I_p^+, I_p^-, I_q^+, and I_q^-). If the angles of PCC and grid voltages are set to be equal, a simple solution for (33) can be
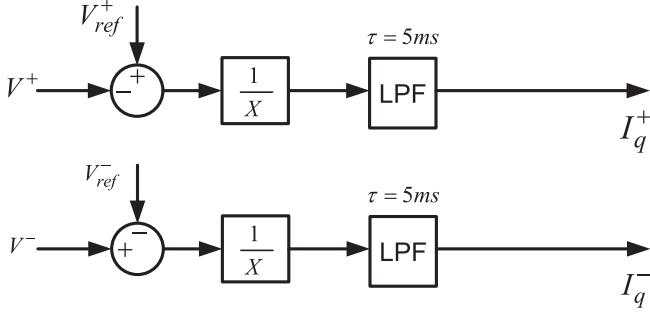
Fig. 2.   VSS based on (35).

obtained as

$$I_p^+ = \frac{R}{X^2 + R^2} \times \Delta V_{\text{ref}}^+$$

$$I_p^- = \frac{R}{X^2 + R^2} \times \Delta V_{\text{ref}}^-$$

$$I_q^+ = \frac{X}{X^2 + R^2} \times \Delta V_{\text{ref}}^+$$

$$I_q^- = \frac{-X}{X^2 + R^2} \times \Delta V_{\text{ref}}^-. \tag{34}$$

For inductive grid impedances, (34) can be simplified into

$$I_p^+ = I_p^- = 0, \; I_q^+ = \frac{\Delta V_{\text{ref}}^+}{X}, \; I_q^- = \frac{-\Delta V_{\text{ref}}^-}{X}. \tag{35}$$

Fig. 2 demonstrates the VSS obtained from (35).

To benefit from both VSS and MAP strategies, combination of both the strategies is proposed in this paper. Hence, the objectives of both strategies are simultaneously accomplished:

1) regulating the phase voltages within the prespecified boundaries,
2) injecting the maximum active power, and
3) respecting the predefined current limit, I_{limit}.

If the X/R ratio of the system is high, the active current components of (34), i.e., I_p^+ and I_p^-, do not contribute significantly in regulating the voltage. In this case, the voltage support should be entirely accomplished by the reactive currents, and the active current components can be used to inject the maximum allowable active power with respect to the current limitation. Therefore, I_q^+ and I_q^- should be determined using the proposed VSS strategy illustrated in Fig. 2. After determining I_q^+ and I_q^-, the amount of Q and k_q can be obtained from

$$Q = I_q^+ V^+ + I_q^- V^-, k_q = \frac{I_q^+ V^+}{Q}. \tag{36}$$

Then, using (18)–(19), the maximum allowable active power is also determined.

V. SIMULATION RESULTS

To demonstrate the effectiveness of the proposed support schemes, five test cases are studied and implemented in this paper. Fig. 3 illustrates the circuit topology of a grid-connected 210 kVA, 690 V, 60 Hz converter-interfaced DG unit. The ac voltage source (grid), line impedances, and the indicated fault in Fig. 3 are used to realize the desired voltage dip presented in Fig. 4(a). A dc power supply can be used to realistically emulate the renewable energy resources and storage in the dc link. This common assumption is widely used in most studies [14]–[20]. It is also assumed that a type B fault (phase A to ground) occurs with a significant voltage dip on phase A, as indicated in Fig. 4(a). The simulation system parameters are listed in Table I. The applied current control system consists of four independent proportional-integrator (PI) controllers in the positive and negative dq-frame to regulate the currents of (2). The parameters of the current controllers (with subscript "cc") and the phase-locked loop controller (with subscript "pll") are also reported in Table I. These controllers are designed based on the well-known methods in this area, such as [3] and [22].

A. Test Case A: Performance Evaluation of the MOP and MOQ Strategies

This section presents the simulation results of two of the proposed strategies: MOP and MOQ. In normal operation, k_p and k_q both are set to be 1, and consequently, pure positive sequence current injection is applied [2]. The results are obtained under the grid faults, where a single-phase-to-ground fault is emulated, and the PCC voltage deteriorates, as indicated in Fig. 4. Between $t_1 = 0.3$ s and $t_2 = 0.6$ s, a moderate voltage dip happens where $V_a = 0.5$ pu. In addition, for more evaluations, a solid one-phase fault is emulated after $t_2 = 0.6$ s where V_a is almost 0. In this test case, P and Q are set to be 100 kW and 30 kvar, respectively. k_p and k_q are obtained according to (13) and (14), not limited to "1". According to Fig. 4, the oscillations on the active and reactive powers are canceled after applying the MOP (at $t = 0.4 - 0.5$ s and $t = 0.7 - 0.8$ s) and MOQ (at $t = 0.5 - 0.6$ s and $t = 0.8 - 1$ s) strategies, respectively.

B. Test Case B: Performance Evaluation of the MFC Strategy

In this test case, the result of the proposed MFC strategy is examined. This test case uses the reference values of Fig. 1(c) for P, Q, and k_q which are 0.4 p.u., 0.7 p.u., and 0.8, re-

$$V_{\text{ref}}^+ = \sqrt{\frac{\lambda_{\max} V_{\min}^2 - \lambda_{\min}(V_{abc-\max}^*)^2 + \sqrt{\left(\lambda_{\max} V_{\min}^2 - \lambda_{\min}(V_{abc-\max}^*)^2\right)^2 - \left(V_{\min}^2 - (V_{abc-\max}^*)^2\right)^2}}{2(\lambda_{\max} - \lambda_{\min})}} \tag{31}$$

$$V_{\text{ref}}^- = \sqrt{\frac{\lambda_{\max} V_{\min}^2 - \lambda_{\min}(V_{abc-\max}^*)^2 - \sqrt{\left(\lambda_{\max} V_{\min}^2 - \lambda_{\min}(V_{abc-\max}^*)^2\right)^2 - \left(V_{\min}^2 - (V_{abc-\max}^*)^2\right)^2}}{2(\lambda_{\max} - \lambda_{\min})}}. \tag{32}$$
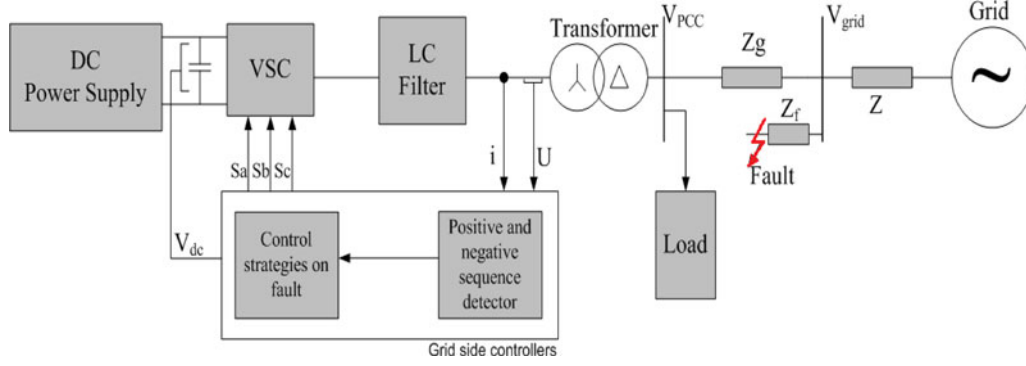
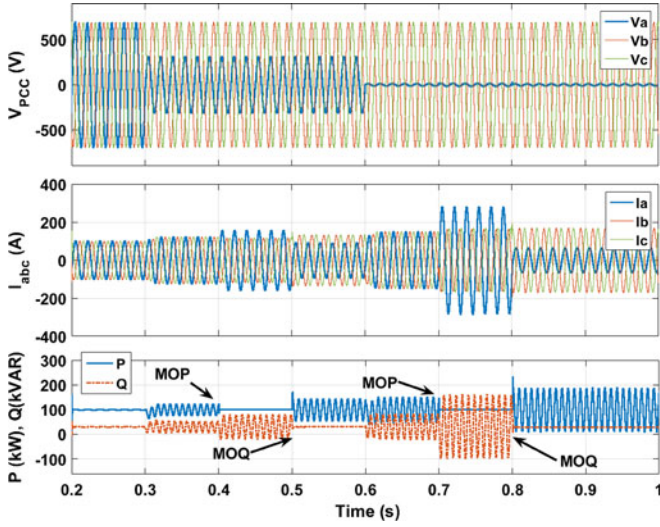Fig. 3. Circuit topology of the GCC.

Fig. 4. Simulation results of MOP and MOQ strategies. From top to bottom: PCC voltage, injected currents, and active/reactive powers.

Fig. 5. Simulation results of MFC strategy. From top to bottom: PCC voltage, injected current, and active/reactive powers.

TABLE I
SIMULATION TEST SYSTEM PARAMETERS

Z_g [Test A and B] $(m\Omega)$	$7 + j34$	Z_g [Test C and D] (Ω)	$j1$
Z $(m\Omega)$	1	$V_{DC}(V)$	2000
Z_f $(m\Omega)$	0.8	$V_{L-L, RMS}(V)$	690
I_{limit} (A)	200	f (Hz)	60
$Kp\text{-}cc$	0.05	$Ki\text{-}cc$	1
$Kp\text{-}pll$	180	$Ki\text{-}pll$	3200

spectively. According to the proposed equations in Section III-C, the optimal k_p value is determined as $k_p = 0.79$ to minimize the fault current. Fig. 5 shows the result of applying the MFC strategy at $t = 0.6$ s.

C. Test Case C: Performance Evaluation of the MAP Strategy

This section examines and studies the proposed equations for the MAP strategy under different fault conditions. The grid voltage becomes deteriorated according to Fig. 6. The values of the Q and k_q are set to the numbers indicated in Fig. 6. Using (17)–(19), the maximum reference P is determined where all three-phase currents are under the preset maximum value for
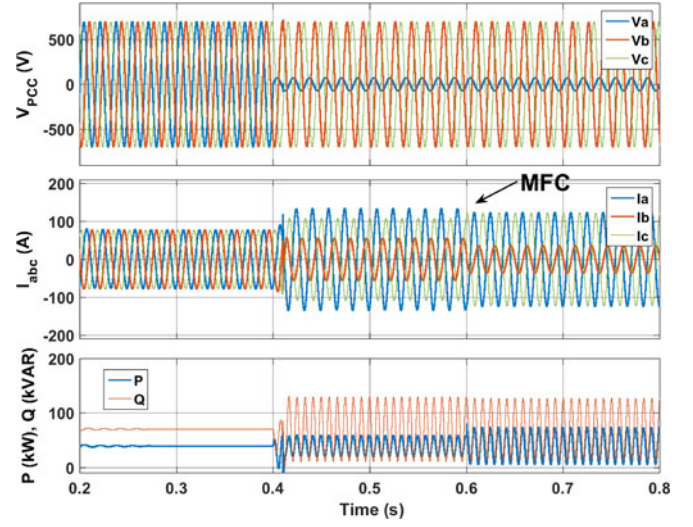
the current. Due to space limitation, the simulation results of the MAQ strategy are not presented here. These results are similar to those of the MAP strategy, except that the maximum reactive power is determined in the MAQ by (20)–(22).

D. Test Case D: Performance Evaluation of VSS-MAP Strategy

This test case shows the performance of the proposed VSS-MAP strategy. Four different voltage sags occur for one phase of the grid voltage at $t = 0.1$, 0.25, 0.4, 0.55 s, respectively. To clearly illustrate the performance of the proposed VSS method, a 0.05 delay is considered after all the fault occurrences to compare the results before and after applying the VSS strategy. Fig. 7 shows that by using this strategy, all three phases are regulated in the desired range of $V_{min} = 0.9$ p.u. and $V_{max} = 1.1$ p.u.. After $t = 0.4$ s, the voltage sag in phase A is 0.25 p.u. (0.15 p.u. below V_{min}), so boosting V_a with 0.15 p.u. by using only the positive reactive current will cause overvoltage in the other two phases. To tackle overvoltage in the other two phases, the VSS strategy is applied to inject the required negative reactive current as well as the positive reactive current
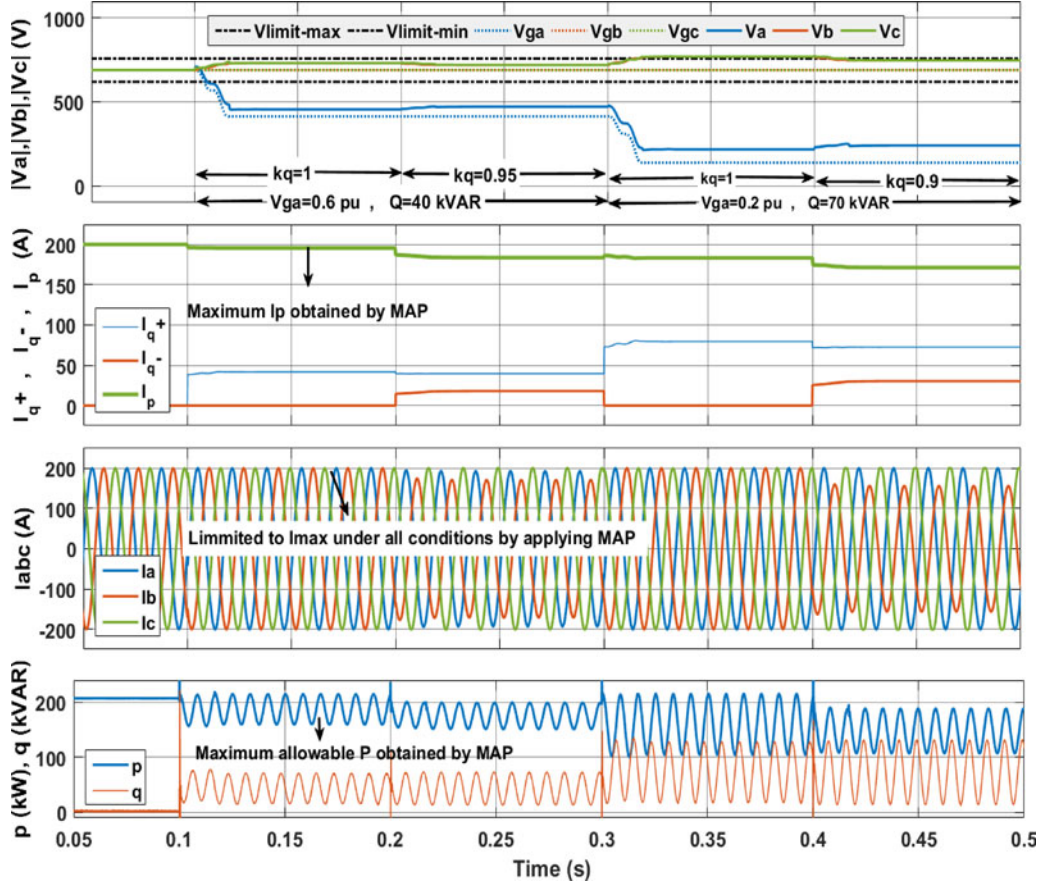
Fig. 6.   Simulation results of MAP strategy. From top to bottom: magnitude of the three-phase voltages injected sequence currents, injected *abc* currents, and active/reactive powers.

[see Fig. 7(b)]. In addition to showing the applied VSS strategy, Fig. 7 demonstrates that the MAP strategy has also determined the maximum active power where the three-phase currents are under the preset limitation, i.e., $I_{\text{limit}} = 200$ A. Therefore, the three objectives of both strategies (as presented in Section IV) are simultaneously accomplished in this test case.

VI. EXPERIMENTAL RESULTS

To verify the analytical expressions and simulation results of the proposed schemes, the experimental test system shown in Fig. 8 is employed. This system contains a VSC connected to the grid and operated in the *PQ* mode. The switching frequency is 10 kHz. The parameters of the test system are reported in Table II. The converter is interfaced to a dSPACE1104 control card via a CMOS/TTL interfacing circuit. The converter is connected to a 60-Hz, 110-V (phase-voltage) three-phase grid via a three-phase transformer. The converter operating voltage is reduced to safely emulate the grid faults and disturbances needed to validate the analytical results. The proposed schemes along with the presented RCG strategy are implemented on the dSPACE1104 supported by a TMS320F240-DSP coprocessor structure for the switching-signal generation. Four PI controllers are designed to regulate the current in the *dq*-frame and positive/negative components.

A. Experimental Test Case A: Performance Evaluation of the MOP and MOQ Strategies

This test case verifies the analytical expressions of (13) and (14), respectively, for the MOP and MOQ strategies. In this test case, $P = 100$ W and $Q = 500$ var are injected by the inverter. An unbalanced fault is created via a fault impedance $(Z_{\text{fault}} = j2\pi f \times 5.1 \, \text{m}\Omega)$ and a circuit breaker, which makes the short circuit between phase *a* and the ground of the system. Fig. 9(a) shows the positive and negative sequences of the voltage during the fault after $t = 1.7$ s. Fig. 9(c) reveals that after the fault occurrence, large oscillations occur on the active and reactive powers. However, the oscillation on the active power is minimized after MOP activation at $t = 5.2$ s.

Fig. 10 shows the experimental results for the MOQ strategy. In this test case, $P = 500$ W and $Q = 100$ var are injected by the inverter. Fig. 10(b) reveals that after the fault occurrence at $t = 2.2$ s, large oscillations exist in the active and reactive powers. The oscillation on the reactive power is minimized after MOQ activation at $t = 5.6$ s.

B. Experimental Test Case B: Performance Evaluation of the MFC Strategy

This test case shows the results of the MFC strategy. In this case, $P = 100$ W and $Q = 175$ var are injected by the GCC, as
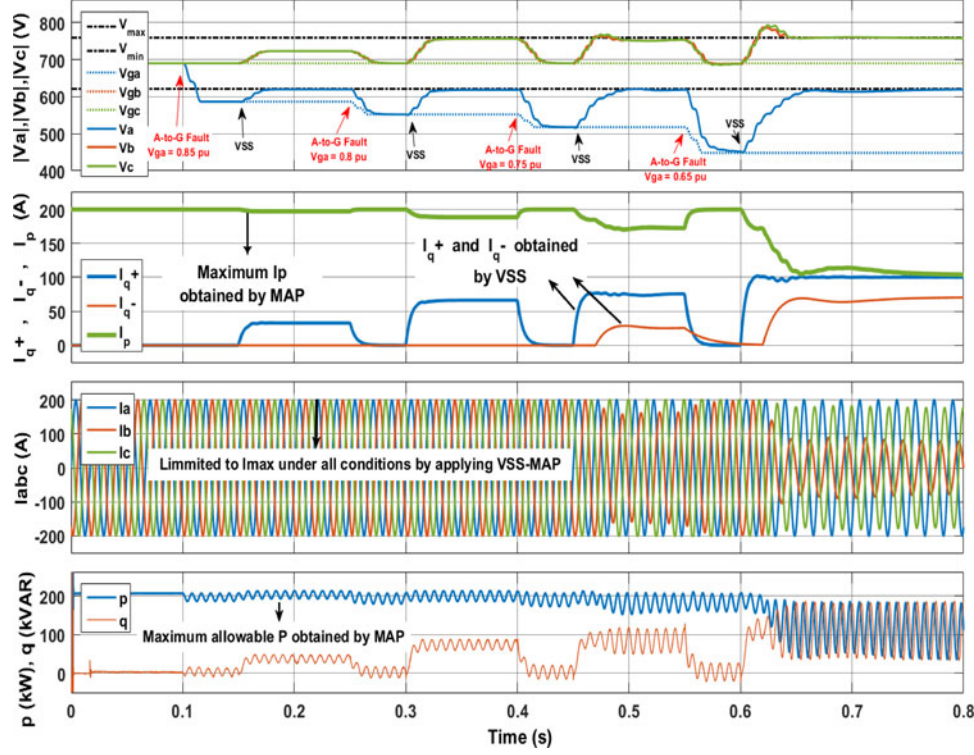
Fig. 7. Simulation results of VSS-MAP strategy: From top to bottom: magnitude of the three-phase voltages injected sequence currents, injected *abc* currents, and active/reactive powers.

Fig. 8. View of the experimental test setup.

TABLE II
EXPERIMENTAL TEST SYSTEM PARAMETERS

Z_g	$j2\pi f \times 1.2\,\mathrm{m\Omega}$	Grid voltage	110 V
Z_{filter}	$j2\pi f \times 4.9\,\mathrm{m\Omega}$	Transformer secondary voltage	35 V
Z_{fault}	$j2\pi f \times 5.1\,\mathrm{m\Omega}$	S	1500 VA
Z	$j2\pi f \times 1.2\,\mathrm{m\Omega}$	I_{limit}	20 A
$Kp\text{-}pll$	5	f	60 Hz
$Kp\text{-}cc$	7.5	$Ki\text{-}cc$	10

three known parameters (i.e., $P = 100$ W, $Q = 175$ VAr, and $k_q = 0.8$) and the characteristics of the fault ($n = 0.25$). The MFC strategy reduces the phase currents to 8 A, as Fig. 11(b) illustrates.

C. Experimental Test Case C: Performance Evaluation of MAQ Strategy

This test case examines the effectiveness of the proposed MAQ scheme. In this test case, $P = 150$ W is injected by the GCC, as shown in Fig. 12(c). A similar phase-to-ground fault occurs at $t = 1.5$ s, as illustrated in Fig. 12(a). Due to this fault, the voltage profile drops from 30 to 25 V (%16.6 voltage drop). At $t=4.3$ s, the MAQ scheme is triggered with the predefined $I_{\mathrm{limit}} = 10$ A, as shown in Fig. 12. In practical applications, this scheme can be triggered automatically and immediately after the fault. However, it is configured manually in this test case to show the results before and after applying the MAQ scheme. According to Fig. 12(a), the PCC voltage is increased to 29 V
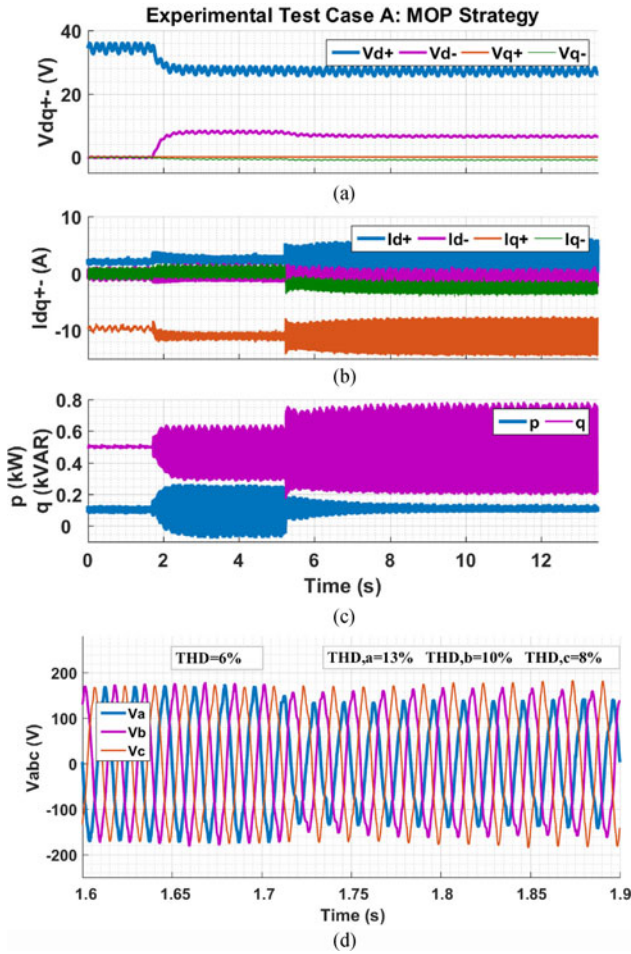
indicated in Fig. 11(c). Again, a similar phase-to-ground fault occurs at $t = 2.6$ s, as shown in Fig. 11(a). In this test case, k_q is taken to be 0.8 after the fault occurrence. After the fault, the phase currents increase up to 9.5 A. At $t = 11$ s, the MFC strategy is activated. The activation changes the value of k_p from 1 to 0.79 to minimize the maximum phase current. Using the MFC strategy, the optimum k_p value is obtained by using the

Fig. 9. Experimental results of the MOP strategy: (a) faulted PCC voltage, (b) currents in the dq^{+-} frame, (c) active and reactive powers, and (d) zoomed view of the *abc* voltages during the fault.
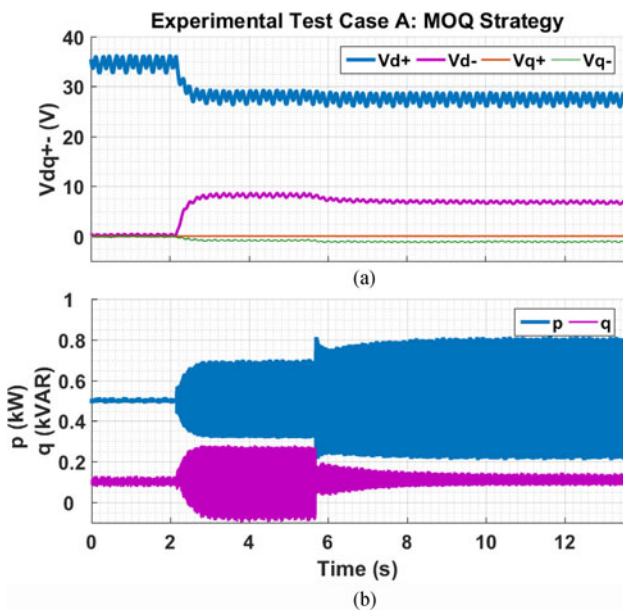

Fig. 10. Experimental results of the MOQ strategy: (a) faulted PCC voltage and (b) active and reactive powers.
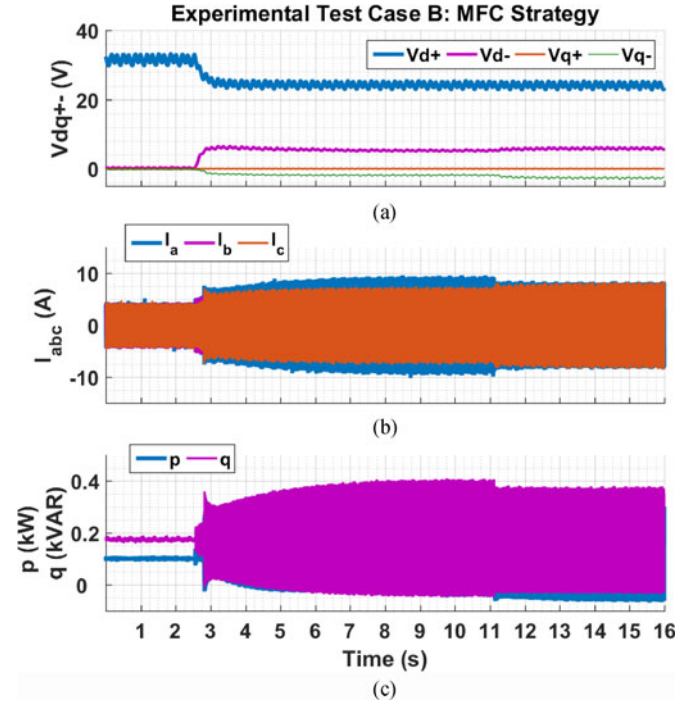

Fig. 11. Experimental results of the MFC strategy: (a) faulted PCC voltage, (b) currents in the *abc* frame, and (c) active and reactive powers.
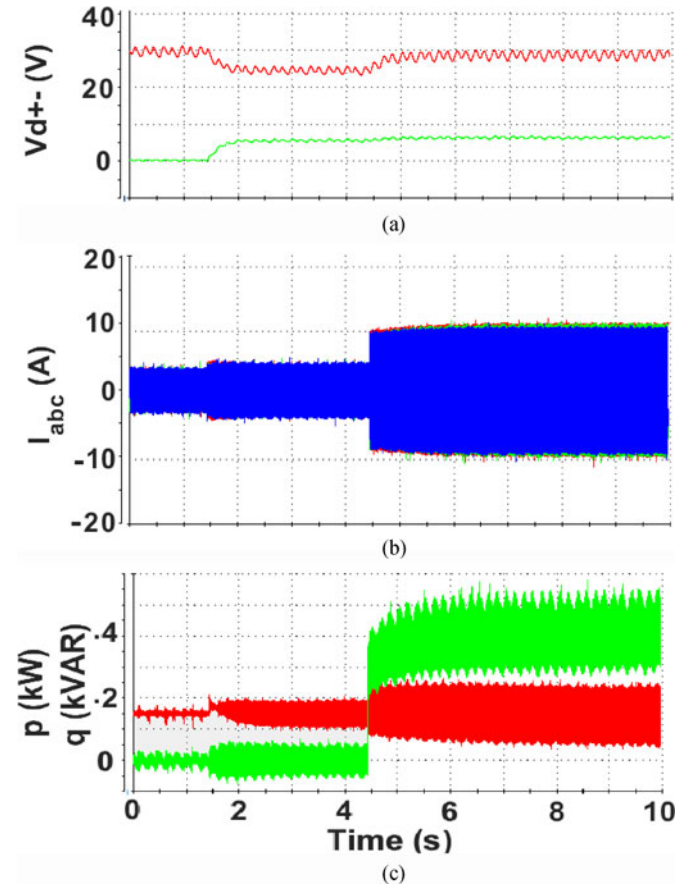

Fig. 12. Experimental results of the MAQ strategy: (a) faulted PCC voltage, (b) currents in the *abc* frame, and (c) active and reactive powers.
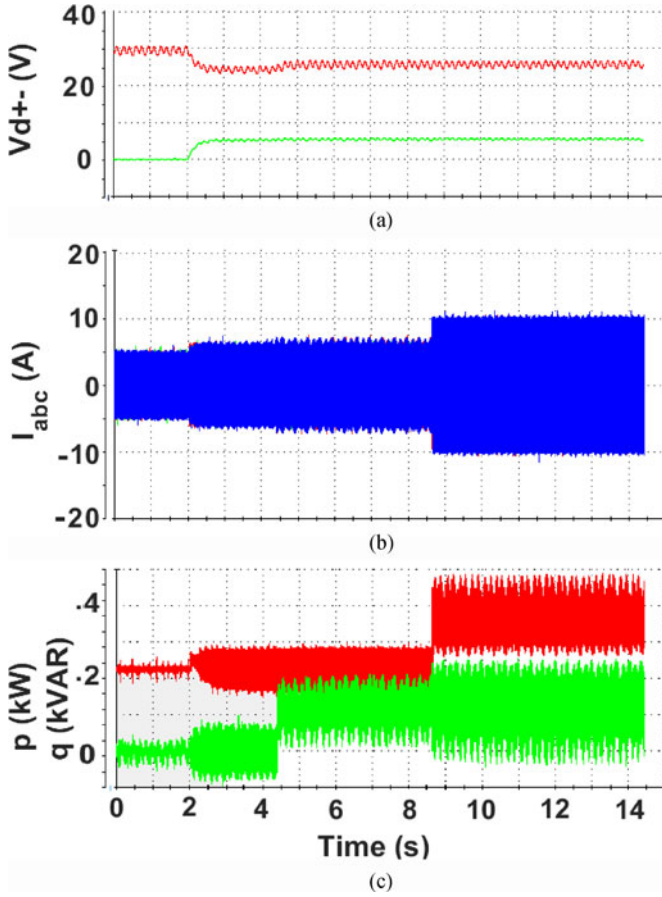
Fig. 13. Experimental results of the MAP strategy: (a) faulted PCC voltage, (b) currents in the *abc* frame, and (c) active and reactive powers.

after applying the MAQ scheme. Also, the injected currents are limited to the predefined $I_{\text{limit}} = 10$ A value, as indicated in Fig. 12(b).

D. Experimental Test Case D: Performance Evaluation of the MAP Strategy

This test case provides the grid code requirement for the Q injection during the low voltage and investigates the application of the MAP strategy. In this test case, $P = 225$ W is initially injected by the GCC, as shown in Fig. 13(c). Similarly, a phase-to-ground fault occurs at $t=2$ s, as shown in Fig. 13(a). This fault causes the PCC voltage to drop from 30 to 25 V. At $t = 4.3$ s, the reactive power imposed by the grid code requirement is injected [9]. This injection causes the PCC voltage to increase to 26 V, as shown in Fig. 13(a). Also, at $t = 8.6$ s, the MAP strategy is activated to inject the maximum allowable active power with respect to $I_{\text{limit}} = 10$ A. As shown in Fig. 13(b), the *abc* currents are limited to 10 A under the unbalanced fault and after applying the MAP scheme.

VII. CONCLUSION

This paper presented optimal reference current generation schemes by injecting a proper set of positive/negative

active/reactive currents using four controlling parameters. Analytical expressions were proposed to find the optimal values of these parameters under any grid voltage condition. The proposed schemes aim to regulate the three-phase voltages, minimize power oscillations, minimize fault currents, and maximize power delivery, under low-voltage and unbalanced condition. These optimal performances have substantial advantages in increasing the penetration level of GCCs, such as improving their efficiency, lowering dc-link ripples, increasing ac system stability, complying with stringent grid codes, and avoiding equipment tripping. The successful results of the proposed schemes were verified using simulation and experimental test results.

REFERENCES

[1] F. Blaabjerg, M. Liserre, and K. Ma, "Power electronics converters for wind turbine systems," *IEEE Trans. Ind. Appl.*, vol. 48, no. 2, pp. 708–719, Mar./Apr. 2012.

[2] M. M. Shabestary, "A comparative analytical study on low-voltage ride-through reference-current-generation strategies in converter-interfaced DER Units," Electr. Comput. Eng. Dept. M.Sc. thesis, Univ. Alberta, Edmonton, AB, Canada, 2015.

[3] R. Teodorescu, M. Liserre, and P. Rodriguez, *Grid Converters for Photovoltaic and Wind Power Systems*. Hoboken, NJ, USA: Wiley, 2011.

[4] T. Vrionis, X. Koutiva, and N. Vovos, "A genetic algorithm-based low voltage ride-through control strategy for grid connected doubly fed induction wind generators," *IEEE Trans. Power Syst.*, vol. 29, no. 3, pp. 1325–1334, May 2014.

[5] D. Xie, Z. Xu, L. Yang, Y. Ostergaard Xue, and K. Wong, "A comprehensive LVRT control strategy for DFIG wind turbines with enhanced reactive power support," *IEEE Trans. Power Syst.*, vol. 28, no. 3, pp. 3302–3310, Aug. 2013.

[6] C. Rahmann, H. J. Haubrich, A. Moser, R. Palma-Behnke, L. Vargas, and M. B. C. Salles, "Justified fault-ride-through requirements for wind turbines in power systems," *IEEE Trans. Power Syst.*, vol. 26, no. 3, pp. 1555–1563, Aug. 2011.

[7] S. Muyeen, R. Takahashi, T. Murata, and J. Tamura, "A variable speed wind turbine control strategy to meet wind farm grid code requirements," *IEEE Trans. Power Syst.*, vol. 25, no. 1, pp. 331–340, Feb. 2010.

[8] A. Mullane, G. Lightbody, and R. Yacamini, "Wind-turbine fault ride-through enhancement," *IEEE Trans. Power Syst.*, vol. 20, no. 4, pp. 1929–1937, Nov. 2005.

[9] Y. Bae, T. Vu, and R. Kim, "Implemental control strategy for grid stabilization of grid-connected PV system based on german grid code in symmetrical low-to-medium voltage network," *IEEE Trans. Energy Convers.*, vol. 28, no. 3, pp. 319–631, Sep. 2013.

[10] A. Hajizadeh, M. A. Golkar, and A. Feliachi, "Voltage control and active power management of hybrid fuel-cell/energy-storage power conversion system under unbalanced voltage sag conditions," *IEEE Trans. Energy Convers.*, vol. 25, no. 4, pp. 1195–1208, Dec. 2010.

[11] T. Vrionis, X. Koutiva, N. Vovos, and G. B. Giannakopoulos, "Control of an HVdc link connecting a wind farm to the grid for fault ride-through enhancement," *IEEE Trans. Power Syst.*, vol. 22, no. 4, pp. 2039–2047, Nov. 2007.

[12] L. Xu, L. Yao, and C. Sasse, "Grid integration of large DFIG-based wind farms using VSC transmission," *IEEE Trans. Power Syst.*, vol. 22, no. 3, pp. 976–984, 2007.

[13] C. Feltes, H. Wrede, F. Koch, and I. Erlich, "Enhanced fault ride-through method for wind farms connected to the grid through VSC-based HVDC transmission," *IEEE Trans. Power Syst.*, vol. 24, no. 3, pp. 1537–1546, Aug. 2009.

[14] J. Miret, A. Camacho, M. Castilla, L. Garc´ýa de Vicuna, and J. Matas, "Control scheme with voltage support capability for distributed generation inverters under voltage sags," *IEEE Trans. Power Electron.*, vol. 28, no. 11, pp. 5252–5262, Nov. 2013.

[15] A. Camacho, M. Castilla, J. Miret, R. Guzman, and A. Borrell, "Reactive power control for distributed generation power plants to comply with voltage limits during grid faults," *IEEE Trans. Power Electron.*, vol. 29, no. 11, pp. 6224–6234, Nov. 2014.

[16] J. Chen, L. Jiang, and W. Yao Wu, "Perturbation estimation based non-linear adaptive control of a full-rated converter wind turbine for fault ride-through capability enhancement," *IEEE Trans. Power Syst.*, vol. 29, no. 6, pp. 2733–2743, Nov. 2014.

[17] P. Rodriguez, A. V. Timbus, R. Teodorescu, M. Liserre, and F. Blaabjerg, "Flexible active power control of distributed power generation systems during grid faults," *IEEE Trans. Ind. Electron.*, vol. 54, no. 5, pp. 2583–2592, Oct. 2007.

[18] K. Ma, W. Chen, M. Liserre, and F. Blaabjerg, "Power controllability of three-phase converter with unbalanced AC source," *IEEE Trans. Power Electron.*, vol. 30, no. 3, pp. 1591–1604, Mar. 2015.

[19] A. Camacho, M. Castilla, J. Miret, J. C. Vasquez, and E. Alarcon-Gallo, "Flexible voltage support control for three-phase distributed generation inverters under grid fault," *IEEE Trans. Ind. Electron.*, vol. 60, no. 4, pp. 1429–1441, Apr. 2013.

[20] X. Guo, X. Zhang, B. Wang, W. Wu, and J. M. Guerrero, "Asymmetrical grid fault ride-through strategy of three-phase grid-connected inverter considering network impedance impact in low-voltage grid," *IEEE Trans. Power Electron.*, vol. 29, no. 3, pp. 1064–1068, Mar. 2014.

[21] H. Akagi, E. H. Watanabe, and M. Aredes, *Instantaneous Power Theory and Applications to Power Conditioning*. Hoboken, NJ: Wiley 2007.

[22] A. Yazdani and R. Iravani, *Voltage-Sourced Converters in Power Systems: Modeling, Control, and Applications*. Hoboken, NJ: Wiley, 2010.

Masoud M. Shabestary (S'14) received the B.Sc. degree in electrical engineering from Amirkabir University of Technology (Tehran Polytechnic), Tehran, Iran, in 2011 and the M.Sc. degree in energy systems in 2015 from the University of Alberta, Edmonton, AB, Canada, where he is currently working toward the Ph.D. degree in electrical engineering.

From 2011 to 2013, he served as a Research Assistant at the FACTS laboratory, Amirkabir University of Technology, Tehran, Iran. His research interests include renewable energy and distributed generation units, their analysis, control and protection, and application of power converters in smart hybrid ac/dc microgrids.

Yasser Abdel-Rady I. Mohamed (M'06–SM'011) was born in Cairo, Egypt, on November 25, 1977. He received the B.Sc. (Hons.) and M.Sc. degrees in electrical engineering from Ain Shams University, Cairo, Egypt, in 2000 and 2004, respectively, and the Ph.D. degree in electrical engineering from the University of Waterloo, Waterloo, ON, Canada, in 2008.

He is currently with the Department of Electrical and Computer Engineering, University of Alberta, AB, Canada, as an Associate Professor. His research interests include dynamics and controls of power converters; grid integration of distributed generation and renewable resources; microgrids; modeling, analysis and control of smart grids; and electric machines and motor drives.

Dr. Mohamed is an Associate Editor of the IEEE TRANSACTIONS ON INDUSTRIAL ELECTRONICS and the IEEE TRANSACTIONS ON POWER ELECTRONICS, and an Editor of the IEEE TRANSACTIONS ON POWER SYSTEMS and IEEE TRANSACTIONS ON SMART GRID. He is a registered Professional Engineer in the Province of Alberta, Canada.